# MILP Algorithm for outlet temperature optimization of a hybrid concentrated solar thermal system for SHIP considering a 1D solar field and a dual phase thermocline storage

**Simon Kamerling[1,2], Valéry Vuillerme[2] and Sylvain Rodat[3]**

[1]Université Savoie Mont-Blanc, USMB(France)
[2]Université Grenoble Alpes, CEA, LITEN, INES, L2TS (France)
[3]CNRS-PROMES (France)

**Abstract**

Solar Heat for Industrial Processes (SHIP) is in an increasing trend in research for industrial decarbonization. Process heat demand and solar energy can both present large intermittencies. Storage gives a degree of freedom on which mathematical optimization can be performed. Lowering the working temperature of the solar field decreases the heat losses and therefore maximizes the production; it also reduces heat losses from the storage while increasing its use in the operational phase. In this paper, the investigated system is a solar field consisting of low-cost Parabolic Trough Collectors in series with Linear Fresnel Receivers, in series with a dual-phase thermocline storage. A MILP (Mixed Integer Linear Programming) algorithm is used in order to obtain a control trajectory of the system; then, this control trajectory is injected in a non-linear and more accurate plant model to evaluate its performances. Comparison is performed with another control approach, consisting in producing at the process temperature whenever possible. The MILP control shows an absolute increase of the solar fraction of 2.5%. The way the thermocline is handled is not standard (as compared to what is done for electricity production) but shows a great interest for heat applications.

*Keywords: MILP, SIPH, SHIP, concentrated solar thermal, concentrated solar heat, operating temperature optimization, flexible heat integration, process heat, storage, system modelling, control strategy, dual-phase thermocline*

## 1. Introduction

Heat, this low exergy energy often discredited in public debates, where electricity has the foreground, represents 50% of the final energy consumed in 2019 (IEA, 2020), with electricity and mobility representing 20% and 30% respectively. Heat production, in 2019, emitted 13.3 Gt-$CO_2$-eq., which corresponds to 40% of total emissions.

Among this 50% of heat, half is used by industrial processes and 47% for heating and domestic hot water, the 3% remaining being for various uses. It is consequently urgent to decarbonize heat for industry if humanity wants to keep the actual level of production without suffering from the consequences. Many renewable solutions allow a decarbonization of heat; the most used today are biomass (~79% of renewable heat in industry), electricity from renewable sources (~10%) and heat from heat networks (~3%). Solar thermal is unfortunately not much used today. Indeed, solar thermal has often been criticized for its price and the space required for its implementation.

In Europe, gas prices are currently under market pressure, having reached €108/MWh in October 2021; the resilience and independence of our industrial systems are thus naturally questioned.

It seems more and more obvious that, for temperate climates and installations in non-desert areas (and, as a result, where space is limited), the solar energy cannot be a unique source of energy along the year. Consequently, it must be hybridized. Hybridization with wind energy, by mechanical wind turbine and Joule effect (Okazaki et al., 2015), as well as biomass, would enable an effective form of resilience to be achieved. Production could be adapted to the availability of energy, if too many external constraints appear in future supplies. Investment in these energies and research is therefore increasingly seen as a modern emergency. We assume in this work that the industry must run at the planned schedule: the heat demand is considered immutable, although some works (Fitsum et al., 2018) showed the interest of managing demand.

In this article, we will discuss the hybridization of a solar field with a boiler. As the boiler operates at high temperature (and thus with higher exergy), it is interesting to reduce the temperature at the exit of the solar field, thus increasing the solar performance and reducing the fuel requirements. This concept of Flexible Heat Integration was proposed by (Rashid et al., 2019). A previous article (Kamerling et al., 2021) has been published


doi:10.18086/swc.2021.29.04 Available at http://proceedings.ises.org

on a similar optimization, with two-tank storage. MILP (Mixed-Integer Linear Programming) algorithms have been widely used in the optimization of solar thermo-electric power plants, such as (Pousinho et al., 2014; Yang et al., 2018).

In this paper, a MILP algorithm is used to obtain a control trajectory, which is then applied to a more complex model, taking into account nonlinearities. The purpose of this paper is to share model developments, considering a 1D solar field and a dual phase thermocline storage.

The first part (section 2) presents the investigated system and the general co-simulation approach used in this paper. The second part describes the implemented solar field and the thermocline 1D models; the third part describes the MILP algorithm and the associated control, as well as an alternative control approach enabling a comparison of the results. In the fourth part, the results of a case study are given.

## 2. Proposed system and modeling approach

### 2.1. System under consideration

#### 2.1.1. Diagram and description of the studied solar concentration system

The system chosen in this study is a solar field consisting of low-cost parabolic trough collectors (PTC) in series with higher efficiency Linear Fresnel Receivers (LFR), the solar field being in series with a thermocline storage, although it is possible to bypass the storage and to go directly to the boiler.

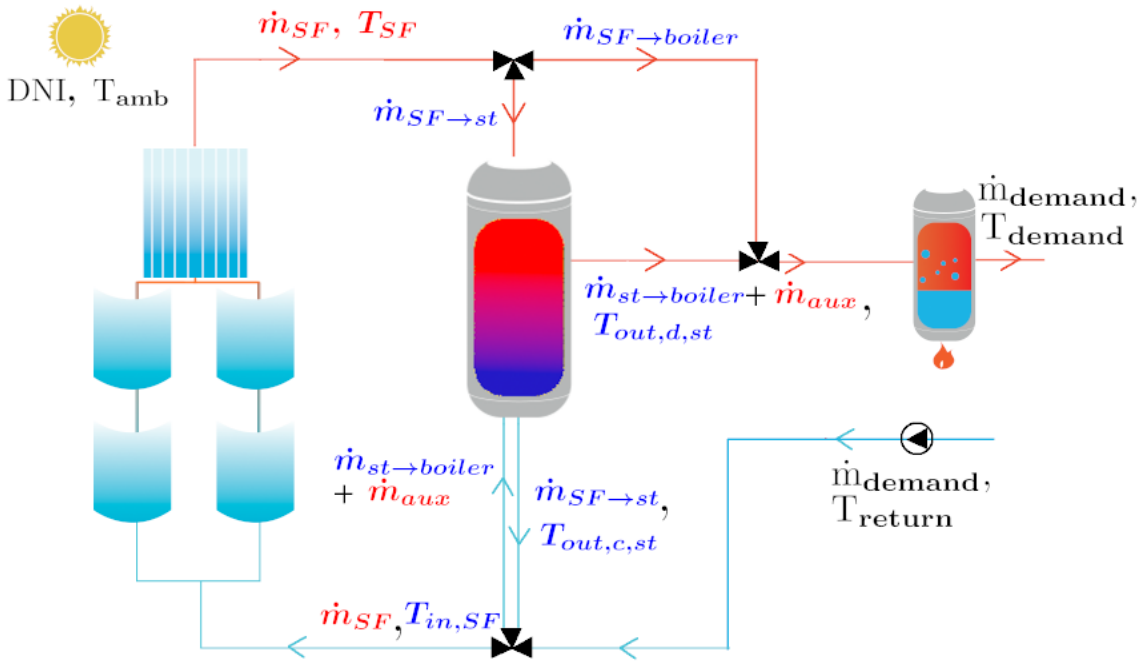


**Fig 1. Diagram of the solar thermal system studied and the variables of interest**

In Figure 1, we can see on the left, the solar field (described in section 3.1); in the middle, the thermocline storage (section 3.2); on the right, the boiler. The variables in black correspond to the input data of the model, those in red correspond to the control trajectory obtained from control algorithms (section 4) and those in blue are deduced from the control trajectory (section 3.3).

The Heat Transfer Fluid (HTF) enters the system with a mass flow rate $\dot{m}_{demand}$, at a temperature $T_{return}$. It has to be sent to the process at the temperature $T_{demand}$, both being constants along the year. If the storage is in discharge mode (outlet temperature $T_{out,d,st}$), some or all of the fluid may enter the thermocline storage; part of this flow ($\dot{m}_{aux}$) comes from the control trajectory, whereas the other part is deduced from the operating mode ($\dot{m}_{st\rightarrow boiler}$). From the point of view of control algorithms, $\dot{m}_{aux}$ allows the solar field to be bypassed. Passing it through storage resets the thermocline. If the storage is in charge mode (outlet temperature $T_{out,c,st}$), part of the

flow comes from the storage $\dot{m}_{SF\rightarrow st}$, which means that the inlet temperature of the solar field $T_{in,SF}$ has to be recalculated, in case the outlet temperature of the storage is significantly higher than the process return temperature $T_{return}$.

#### 2.1.2. Main assumptions

Different assumptions and approximations have been made in this model: the main objective is to compare the different control approaches:

- the quality of the forecast: this is not taken into account, i.e. the meteorological data are assumed to be known in advance. This means, *de facto*, that we are on a probabilistic trajectory corresponding to the median of the probabilities. One way to overcome this assumption would be to use Robust MILP algorithms, such as (He et al., 2016), which allows taking into account the quality of the forecast and making decisions upon the robustness of the solution,
- constant efficiency of the boiler (taken at 100%): this assumption is very accurate in a wide range of operation, the value of 100% is taken as it does not influence the results presented here,
- solar modules' inertia is taken as the contained fluid's inertia,
- no headers were considered in this study, although they add some inertia to the system,
- the chosen HTF is Therminol 66, and its properties are all taken at 1 bar; dependence on temperature is taken into account through interpolation of fluid properties,
- time discretization is hourly.

### 2.2. Modelling approach

Figure 2 shows the modelling approach followed by the algorithm. To calculate the outcomes over the year, a loop is performed every 24h.

Before entering the loop, the algorithm reads the input data, and chooses the design if specified. The outlet temperatures of the solar field are discretized.

At the beginning of the loop, the solar field model calculates the producible mass flow for the different discretized temperatures, considering inertia.

Then, an optimization algorithm chooses the optimal control trajectory upon 48h. The control trajectory is then fed into the non-linear model, which then calculates the heat production and boiler requirements, as well as the storage state and other variables of interest (in blue in Fig.1.), upon 24h. Both storage and solar field final states are then passed as input to the loop. The optimization is run over 48h in order to optimize the storage dispatch for the next day as well (else, the storage is just emptied by the optimization algorithm).

This kind of control strategy is commonly referred to as Rolling Horizon (Moretti et al., 2021).

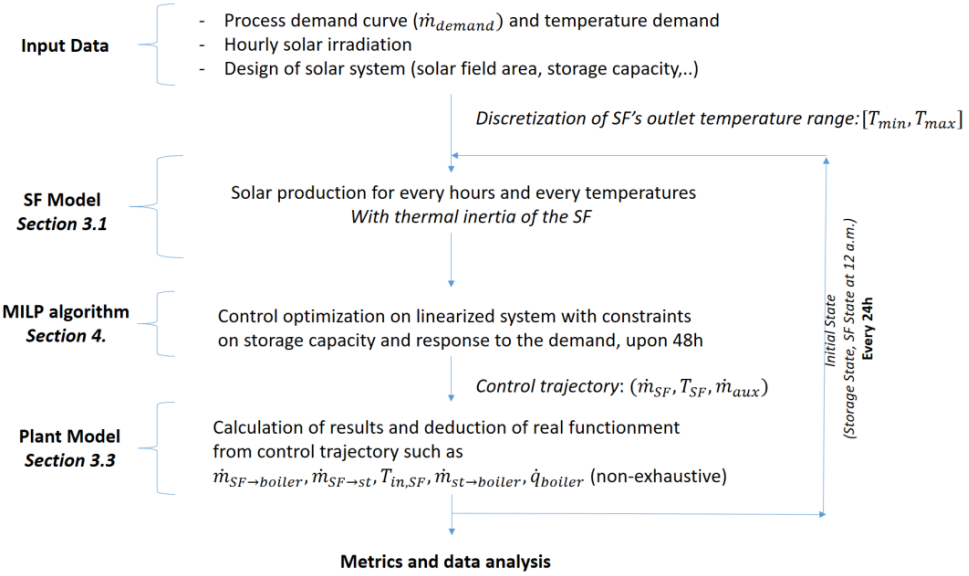


**Fig. 2. Algorithm structure**

# 3. 1D Models

3.1. Solar Field Model

In the present study, the solar field consists of low-cost Parabolic Trough Collectors (from Absolicon) followed by Linear Fresnel Receivers (from Industrial Solar), permitting to reach higher temperatures. This association allows some installations to gain on the cost of the heat produced (FriendSHIP, 2021).

The solar field is modelled in one dimension, with calculations on each module, and this in a quasi-static approach: a stationary calculation is made, then the thermal inertia is translated into a loss or a gain in terms of mass flow, in the manner of the SAM model (Wagner and Gilman, 2011).

Fluid properties are obtained by interpolation. They are assumed to only depend on the temperature.

3.1.1. Optical efficiency and thermal losses

The calculation of the optical efficiency is done in two different ways depending on the collector technology:

- The PTC *via* a longitudinal $IAM_{L,PTC}$ (Incidence Angle Modifier), multiplied by the cosine of the longitudinal angle : $\eta_{opt}(\theta_L) = \eta_{0,PTC} * IAM_{L,PTC}(\theta_L) * \cos(\theta_L)$
- The LFR *via* a longitudinal $IAM_{L,LFR}$ and a transversal $IAM_{T,LFR}$, in which is already included the cosine effect: $\eta_{opt}(\theta_L, \theta_T) = \eta_{0,LFR} * IAM_{L,LFR}(\theta_L) * IAM_{T,LFR}(\theta_T)$

With $\theta_L$ and $\theta_T$ the longitudinal and transversal angles respectively, and $\eta_0$ the optical efficiency at normal incidence, with subscripts corresponding to the concerned module. The end losses are not taken into account, although they are probably significant in the case of small or medium size installations, located in latitudes corresponding to continental Europe. The module incident energy is then written as: $\dot{q}_{in} = G_b * \eta_{opt}(\theta_L, \theta_T) * A_{collector}$, with $G_b$ the beam irradiation in $W.m^{-2}$ and $A_{collector}$ the aperture area in m² of a module.

The heat losses are written in a general way: $\dot{q}_{losses}(\Delta T) = A_{collector} * \sum_{i=1}^{4} a_i \Delta T^i$, with: $\Delta T = \frac{T_{in}+T_{out}}{2} - T_{amb}$ being the average fluid temperature difference with the ambient, $T_{in}$ being the inlet temperature of a module, $T_{out}$ the outlet temperature and $T_{amb}$ the ambient temperature. The $a_i$, $i \in [\![1;4]\!]$ are the heat loss coefficients (from correlations) and are in $W.m^{-2}.K^{-i}$.

3.1.2. Stationary calculation of the outlet temperature of a loop

Knowing the mass flow rate and the inlet temperature, and after calculating the optical efficiency, the outlet temperature of a module is calculated by solving the following equation:

$\dot{m} * C_p * (T_{out} - T_{in}) = \dot{q}_{in} - \dot{q}_{losses}$ (1),

with $\dot{m}$ the mass flow rate in $kg.s^{-1}$ , $C_p$ the fluid specific heat capacity in $J.kg^{-1}.K^{-1}$, $T_{in}$ and $T_{out}$ being respectively the inlet and outlet HTF's temperatures in the SF. This equation is a quartic equation in $T_{out}$. The fluid properties are taken at the inlet temperature.

The calculation of all temperatures in the loop is then performed from one module to another, considering for the module n the outlet temperature of the module n-1.

3.1.3. Quasi-static calculation of the mass flow rate

The output temperature being fixed, the calculation is done in two steps: first, the stationary mass flow rate is calculated, by dichotomy on the outlet temperature, *via* Eq.(1). Then, the energy needed to heat the content of the modules (thermal inertia) to reach their temperature is accounted for, and converted to a mass flow rate before being subtracted from the stationary flow. This is calculated as follows:

$E_{inertia} = \sum_i V_i * \rho(\bar{T}_{i,h}) * \left(h(\bar{T}_{i,h}) - h(\bar{T}_{i,h-1})\right)$ (2) ,

with $V_i$ the HTF volume contained in module i in $m^3$, $\rho$ the density in $kg.m^{-3}$, $h$ the enthalpy of the HTF in $J.kg^{-1}$, $\bar{T}$ the average temperature of the module (calculated by averaging inlet and outlet temperatures), the subscripts h and h-1 referring to the time h and h-1.

The conversion to mass flow rate is then done in the following way: $\dot{m}_{inertia} = \frac{E_{inertia}}{h(T_{SF})*3600}$ (3)

The mass flow rate of the solar field is then written $\dot{m}_{SF} = \dot{m}_{stationary} - \dot{m}_{inertia}$ (4).

3.1.4. Validation

The validation of the solar field 1D model was done using the "Linear Fresnel with Molten Salt" model of the open-source software SAM. Using SAM inlet and outlet temperatures, the hourly mass flow rates were calculated with the above model and compared to SAM's hourly mass flows.

The average relative error of the daily energy production is 2.6% - highest peaks in relative error occur when the daily production is very low. The average relative error on the hourly flow rate is 6.9%. The main reason for the deviations is that in SAM the molten salt/water heat exchanger before entering the turbine has a large thermal inertia, while there is no heat exchanger in the present model. Figure 3 shows the daily heat output of the two models, as well as the relative error between both.

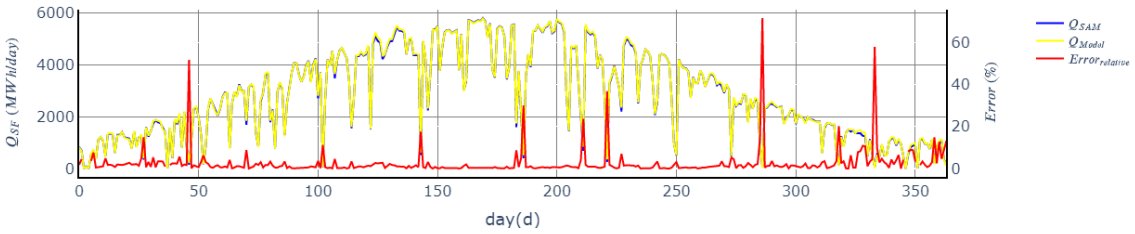


**Fig.3 : Daily heat production of SAM model (yellow) and the model presented here (blue), with relative error in % on the right (red)**

3.1.5. Definition of defocusing

Defocusing has been defined in two ways: firstly, defocusing in series, i.e. in a loop, in order not to exceed the maximum temperature of a collector or not to exceed the output temperature. The defocusing fraction is then defined by: $defocus_{Serie} = \frac{A_{defocalised}}{A_{loop}}$ (5)

Then the parallel defocusing, which consists in defocusing a certain number of loops, in order not to exceed a certain mass flow (full storage, etc.). It is calculated as a ratio between the chosen mass flow and the one that can be produced at the desired outlet temperature: $defocus_{//} = 1 - \frac{\dot{m}_{SF}}{\dot{m}_{possible}}$ (6).

Note that the real defocus is not continuous; however, we are working on a large solar field, which makes the approximation acceptable.

3.1.6. Input parameter values

**Table 1. Parameters of the PTC**

| Parameter (unit) | Value | Description |
|---|---|---|
| $\eta_0$ | 0.697 | Optical efficiency at normal incidence |
| $A_{collector}$(m²) | 5.51 | Collector surface area |
| $a_1(W.m^{-2}.K^{-1})$) | 0.73 | Heat losses coefficient |
| $\dot{m}_{nom}(kg.s^{-1})$ | 0.126 | Nominal mass flow rate |

**Table 2. Parameters of the LFR**

| Parameter (unit) | Value | Description |
|---|---|---|
| $\eta_0$ | 0.686 | Optical efficiency at normal incidence |
| $A_{collector}$(m²) | 30.45 | Collector surface area |
| $a_1(W.m^{-2}.K^{-1})$ | 0.033 | Heat losses coefficient |
| $a_4(W.m^{-2}.K^{-4})$ | 1.48e-9 | Heat losses coefficient |
| $\dot{m}_{nom}(kg.s^{-1})$ | 0.6 | Nominal mass flow rate |

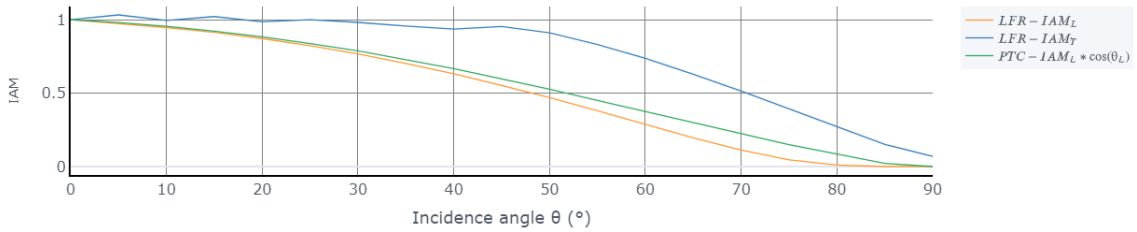


**Fig.4. IAM of the collectors – transversal IAM of the LFR (blue), longitudinal IAM of the LFR (yellow), longitudinal IAM multiplied by cosine of the longitudinal angle of the PTC (green)**

3.2. Dual-phase thermocline

It was chosen to work with a dual-phase thermocline because this storage is cheap, as it consists of only one tank and a large proportion of the often expensive HTF is replaced by a low-cost solid.

3.2.1. Implemented model description

The thermocline model implemented is the one of a dual-phase thermocline, from (Hoffmann et al., 2016), with the correlations from (Esence et al., 2019). It is a model with three partial differential equations: one for the fluid temperature, one for the solid temperature and one for the wall temperature. The resolution of this system involves a one-dimensional discretization over the tank's height. The discretization chosen for the convection term depends on the fluid flow direction:

- Downwind differencing scheme for tank's discharge (rising fluid): $u\frac{\partial T}{\partial x} = u * \frac{T_j - T_{j-1}}{\Delta x}$
- Upwind differencing scheme for tank's charge (dropping fluid): $-u\frac{\partial T}{\partial x} = -u * \frac{T_{j+1} - T_j}{\Delta x}$

The use of the QUICK scheme would be preferable in general cases, but the above formulation is sufficient to have a convergence of the model with liquid fluids. The time discretization is implicit, because the explicit discretization showed very quickly a divergence in the results.

The model is solved using the open-source library *DAE-CPP* (Ikorotkin, 2019), itself based on the free IBM library *Math Kernel Library.*

3.2.2. Validation

This model has been validated with an in-house code, itself validated on experimental data from the STONE installation at CEA Grenoble (Esence et al., 2017).

The validation was done in the following way: a sequence of charges and discharges at different temperature levels were simulated in both models, then a calculation of the temperature difference was done using interpolations, in order to measure the deviation due to the numbers of elements:

$$err = \frac{1}{\Delta t} * \frac{1}{L} * \int_0^L \int_0^{\Delta t} \frac{|T_{ref}(z,t) - T(z,t)|}{T_{ref}(z,t)} dt\, dz$$

For a number of elements equal to 100 (the reference number of the in-house model), we found a difference of 0.9%. For 50 elements, this difference rises to 2.6%, but we have chosen to work with 50 elements as the computation time of the storage depends strongly on this parameter.

Nonetheless, varying the temperature at the inlet (as done further) can create modelling inaccuracies, as the stratification may be disturbed; furthermore, this model does not take into account buoyancy. This would need a deeper modelling for better validation.

3.2.3. Calculation of a threshold HTF mass

Hot fluid should not be sent back in the solar field. There should therefore be a temperature threshold, traduced as an HTF injected mass threshold which should not be exceeded by the control trajectories. This mass is not obvious as the thermocline is filled with solid particles. Taking the temperature threshold as: $T_{threshold} = T_{discharge} + \frac{1}{3}(T_{charge} - T_{discharge})$, a serie of simulations (charge mode) with a constant mass flow rate showed

that the HTF mass threshold that could be injected to reach the temperature threshold was about $M_{threshold} = \rho_{HTF} * V_{tank}$. This result does depend on the mass flow rate but appeared to be a good enough value.

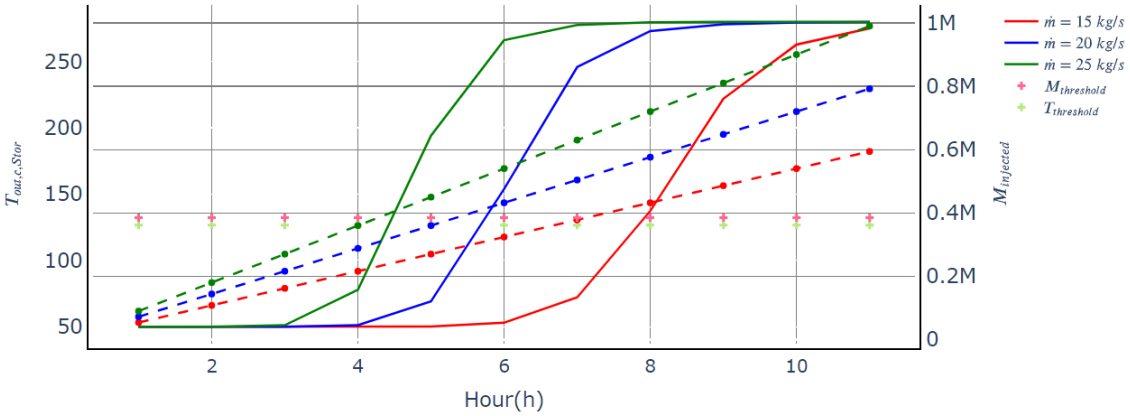


**Fig.5. Storage outlet temperature (continuous line) during a load, with three different mass flow rates; mass injected into the storage (dashes), with the colours corresponding to the flow rates; $M_{threshold} = \rho_{HTF} * V_{tank}$ with the pink crosses; and $T_{threshold}$ with the green crosses**

Figure 5 shows the outlet temperature of the storage under charging, at a constant mass flow rate, for a storage volume equal to 465 $m^3$. The second vertical axis indicates the mass injected into the storage. It can be seen that the storage outlet temperature increases by about 1/3 of the temperature difference when a mass of $M_{thresgold} = \rho_{HTF}(T_{hot}) * V_{tank}$ has been injected in the storage. This remains dependent on the mass flow rate and not perfectly precise.

3.2.4. Definition of the charge percentage

The energy contained in the storage is defined as:

$$E_{storage} = \int_0^L (\epsilon * \rho_{HTF}(T_{HTF}(z)) * h_{HTF}(T_{HTF}(z)) + (1-\epsilon) * \rho_{solid} * h_{solid}(T_{solid}(z)) * A_{tv} dz \quad (7)$$

With $\epsilon$ the rock bed global void fraction, $\rho, h, T$ the density, enthalpy and temperature respectively, the subscripts HTF and solid referring to the different materials involved, and $A_{tv}$ the cross-sectional area of the tank.

By defining $E_{max}$ the stored energy when $\forall z, T_{HTF}(z) = T_{solid}(z) = T_{process}$ and by defining $E_{min}$ the stored energy when $\forall z, T_{HTF}(z) = T_{solid}(z) = T_{return}$, we can define the charge percentage $\tau = \frac{E_{storage} - E_{min}}{E_{max} - E_{min}}$ (8).

3.2.6. Input parameters

**Table 3. Parameters of the dual phase thermocline**

| Parameter (unit) | Value | Description |
|---|---|---|
| $\epsilon$ (-) | 0.27 | Rock bed global void fraction/ HTF Volumetric fraction |
| $d_p$(m) | 0.015 | Equivalent diameter of solid particles |
| $U_{eq}$(W/m².K) | 0.1 | Heat losses coefficient |
| $e_{wall}$(m) | 0.012 | Thickness of the metal wall |
| $C_{p,solid}$ & $C_{p,wall}$(J/kg.K) | 900 & 500 | Specific heat capacity of the solid filler and the wall's metal |
| $\rho_{solid}$ & $\rho_{wall}$(kg/$m^3$) | 2500 & 7200 | Density of the solid and the wall |
| $k_{solid}$ & $k_{wall}$(W/m.K) | 5 & 20 | Thermal conductivity of the solid and the wall |
| $N_{discr}$ | 50 | Number of elements of the thermocline's discretization |

3.3. System model

In this section, the solar thermal system response to the control trajectory is explained; this latter is therefore assumed to be known, i.e., $(\dot{m}_{SF}, T_{SF}, \dot{m}_{aux})$.

**Determination of the storage operating mode**

The mass flow rate of the demand must be assured, which gives:

$$\dot{m}_{demand} = \dot{m}_{SF\rightarrow boiler} + \dot{m}_{st\rightarrow boiler} + \dot{m}_{aux} \quad (10)$$

The flow coming from the solar field can go either to the storage or to the boiler, which gives:

$$\dot{m}_{SF} = \dot{m}_{SF\rightarrow boiler} + \dot{m}_{SF\rightarrow st} \quad (11)$$

We can then write the variation of the inlet and outlet mass flow of the storage:

$$\Delta\dot{m} = \dot{m}_{SF\rightarrow st} - \dot{m}_{st\rightarrow boiler} \quad (12)$$

The reinjection of Eq.(10) and Eq(11) in Eq(12) gives:

$$\Delta\dot{m} = (\dot{m}_{SF} - \dot{m}_{SF\rightarrow boiler}) - (\dot{m}_{demand} - \dot{m}_{aux} - \dot{m}_{SF\rightarrow boiler}) = \dot{m}_{SF} + \dot{m}_{aux} - \dot{m}_{demand} \quad (13)$$

The sign of $\Delta\dot{m}$ then gives the operating mode of the storage.

**Case 1: Storage load: $\Delta\dot{m} > 0$**

It can be deduced that $\dot{m}_{st\rightarrow boiler} = 0$, and thus from Eq.(12) that $\dot{m}_{SF\rightarrow st} = \Delta\dot{m}$. Moreover, one must then necessarily have $\dot{m}_{aux} = 0$, because no control model attempts to load the storage while not producing at least the demand mass flow rate.

We deduce from Eq.(12) and Eq.(13) that $\dot{m}_{SF\rightarrow boiler} = \dot{m}_{SF} - \dot{m}_{SF\rightarrow st} = \dot{m}_{demand}$.

The outlet temperature of the storage is then calculated according to $\dot{m}_{SF\rightarrow st}$, which gives us an outlet temperature of the storage, noted $T_{out,c,st}$. The inlet temperature of the solar field can then be calculated:

$$T_{in,SF} = \frac{\dot{m}_{SF\rightarrow st} * T_{out,c,st} + \dot{m}_{demand} * T_{return}}{\dot{m}_{SF\rightarrow st} + \dot{m}_{demand}} \quad (14)$$

This last one can be quite high if the thermocline zone starts to exit the tank. This is why a mass threshold should be set for those control models. Nonetheless, verification is performed, as well as reactualization of mass flow rates:

- If $T_{in,SF} + 10°C$ is higher than the outlet temperature of the solar field, an attempt is made to run the solar array at the demand temperature, and the flow rates are updated accordingly. Note that this shows a flaw in the control trajectory.
- If not, we recalculate the production of the solar field. If the calculated flow is lower than the flow of the trajectory $\dot{m}_{SF}$, the latter is lowered, and the mass flows are updated. If the calculated mass flow rate is greater than the trajectory mass flow rate $\dot{m}_{SF}$, this is considered as parallel defocusing.

**Case 2: Storage discharge: $\Delta\dot{m} < 0$**

We then deduce that $\dot{m}_{SF\rightarrow st} = 0$, and thus that $\dot{m}_{st\rightarrow boiler} = -\Delta\dot{m}$. It was chosen, given the thermocline type of storage, that $\dot{m}_{aux}$ goes through the thermocline storage (see section 2.1), in order to reset the thermocline and recover a maximum of energy.

The mass flow rate through the storage to the boiler ($\dot{m}_{st\rightarrow boiler}$) becomes:$-\Delta\dot{m} + \dot{m}_{aux}$ .The storage outlet temperature is then determined by the thermocline model; it is noted $T_{out,d,st}$.

**Case 3: Storage inactivity: $\Delta\dot{m} = 0$**

In this case, the control system does not discharge the storage, and we have: $\dot{m}_{SF} = \dot{m}_{SF\rightarrow boiler}$ and $\dot{m}_{demand} = \dot{m}_{aux} + \dot{m}_{SF}$. Due to the implemented logic of thermocline's reset, i.e., that $\dot{m}_{aux}$ passes through the storage, we take: $\dot{m}_{st\rightarrow boiler} = \dot{m}_{aux}$.

The storage outlet temperature is then determined by the thermocline model.

From this data, the boiler requirement is deduced:

$$\dot{q}_{boiler} = \dot{m}_{SF\rightarrow boiler} * \left(h\left(T_{process}\right) - h(T_{SF})\right) + \dot{m}_{st\rightarrow boiler} * \left(h(T_{process}) - h(T_{out,d,st})\right) \quad (15)$$

# 4. Control models

Two control approaches are considered: one from MILP optimization and one from a simple control approach so that the benefit of the MILP algorithm can be evaluated.

## 4.1. MILP algorithm

For the sake of brevity, it was chosen not to expose the full MILP algorithm here, as it may be found in (Kamerling et al., 2021). Nonetheless, a summary is given here, as well as the thermocline specific approach. The cost function is the boiler use. The implemented constraints represent the constraints of the system.

This MILP algorithm can be considered as a *water-flow* MILP, as opposed to *energy-flow* MILP. (Moretti et al., 2021) summarizes well the difference: the second approach only considers energy balances without taking into account temperatures and mass flow rates, whereas the first one directly implements mass flows and temperatures; the non-linear term formed by the product of mass flow rate and temperature is linearized through the use of binary variables and a discretization of the temperature levels, as is described below.

The main subtlety lies in the pre-calculation of the solar field flows at discretized output temperatures, and the use of binary variables for the choice of production. Since inertia must be taken into account, a binary variable spanning two time slots is considered:

$z_{h,i,j} = \begin{cases} 1 \; if \; T_{SF,h} = T_i \; and \; T_{SF,h-1} = T_j \\ 0 \; else \end{cases}$, with $T_i$ and $T_j$ in the set of discretized variables.

The mass stored by the algorithm must not exceed a maximum mass, which we have defined by $M_{max} = \rho_{HTF}(T_{process}) * V_{tank}$, in order not to overpass a threshold temperature at the bottom of the storage, and not to send a too hot fluid in the solar field (see section 3.2.3.).

The notion of bypass flow ($\dot{m}_{aux}$) is necessary because of the MILP algorithm: the thermal losses in the tank must be taken into account to get closer to the real operation, which forces to add in the cost function a cost proportional to the mass in the storage (virtual in the case of a thermocline storage). Therefore, this mass cannot be negative, even though it is virtual. Therefore, it is necessary to define an exit gate to the MILP to respect the constraint of a positive mass.

This is written by the following constraints: $\forall h, 0 \leq M_{st,h} \leq M_{max}$ et $M_{st,h+1} = M_{st,h} + 3600.*(\dot{m}_{SF} + \dot{m}_{aux} - \dot{m}_{demand})$.

The mass present in the storage at the beginning of the MILP calculation (i.e., at midnight), was calculated as follows: $M_0 = M_{max} * \tau$, with τ the charge percentage of the storage defined in 3.2.4.

## 4.2. Control approach 1 (CA1)

This control approach tries to always operate at the process temperature. It therefore heats the solar field in the morning and then switches it on. If the mass flow rate producible at the demand temperature is higher than the demand mass flow rate, the excess is stored. If it is lower, the storage is emptied; if the storage is empty, the bypass flow $\dot{m}_{aux}$ allows to complete the need. If the storage is full, in the sense that the overall mass injected into the thermocline storage is greater than $M_{max}$, the solar field is defocused. The mass present in the storage at the beginning of the simulation is calculated in the same way as above.

# 5. Case Study

A case study is presented here: production of chemical and intermediate products at Tarragona (Spain). The demand is considered constant at 280°C, with a flow rate of 20 kg/s. The return temperature is assumed to be 50°C. This corresponds to a power demand of 11.4 MW, and a daily heat demand of 273.6 MWh. The storage is designed to deliver heat for 6 hours at nominal rate and process temperature. The meteorological data are from PVGIS (EU SCIENCE HUB, 2017). The number of discretization of the outlet temperature of the solar field is 8. The yearly simulation time is of 23 minutes on a computer with a 3GHz processor and 32Go of RAM.

## 5.1. Design

The design of the plant is as follows:

- A loop structure consisting of a "rectangle" of PTC: 10 in series and 5 in parallel, followed by a line of LFR: 8 in series, 1 in parallel. This gives an aperture area for a loop of 519m².
- 67 loops, for a total aperture area of 34.773m²
- A storage volume of 256$m^3$, which makes an HTF volume of 69 $m^3$ and a solid volume of 187$m^3$ , or 56.8t of HTF and 467t of solids, for a storage capacity between $T_{return} = 50°C$and $T_{process} = 280°C$ of $\Delta E = E_{max} - E_{min} = 34.18\ MWh$

5.2. Hourly results

In this section, hourly results are commented. These results correspond to February 25th and 26th, and June 19th and 20th, to compare two different solar conditions.

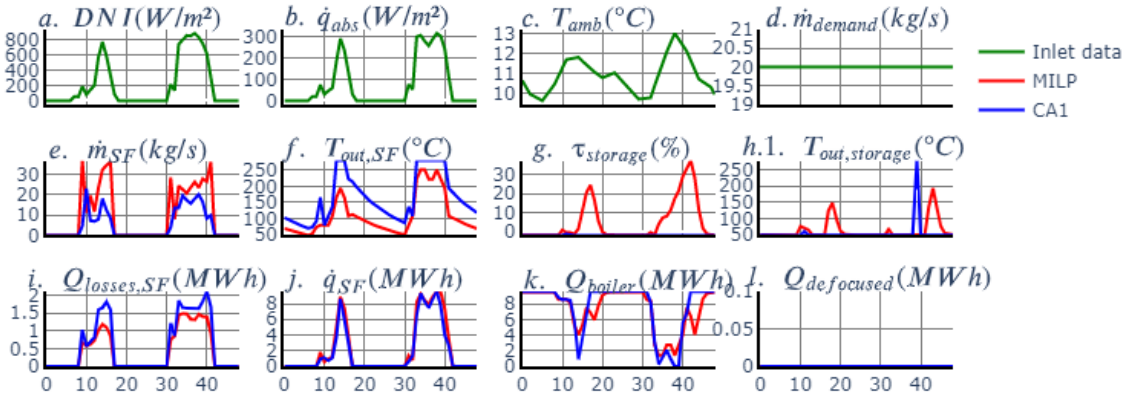


**Fig. 6. Hourly results of the simulation on the 25th and 26th of February**

Fig. 6.a presents the DNI in W/m² which is intermittent on the 25th and closer to a clear-sky day on the 26th; Fig 6.b. shows the power on the receiver, in $W/m^2_{aperture}$; Fig.6.c. gives the ambient temperature in °C; Fig. 6.d. shows the demand mass flow rate in kg/s; Fig.6.e. presents the mass flow rate from both control strategies, i.e. MILP and CA1; Fig.6.f. presents the outlet temperature of the Solar Field; Fig.6.g. presents the stored energy in %; Fig.6.h. presents the outlet temperature of the storage; Fig.6.i. presents the heat losses in the solar field; Fig.6.j. shows the heat collected by the solar field; Fig.6.k. shows the heat produced by the boiler; Fig.6.l. presents the defocused energy in the Solar Field.

Fig.6.e. shows that the mass flow rate is increased in MILP strategy, whereas its outlet temperature is decreased. This explains why the heat losses are lower in the Solar Field, as can be seen on Fig.6.i, as compared to CA1. Fig.6.k. shows that the MILP algorithm smooths the boiler energy need, which is a side effect (i.e., it was not implemented straightforward) that might be interesting if the variability of the efficiency of the boiler with the thermal load is taken into account. Figures 6.g. et 6.h. show that the MILP makes a better use of the storage as compared to CA1.

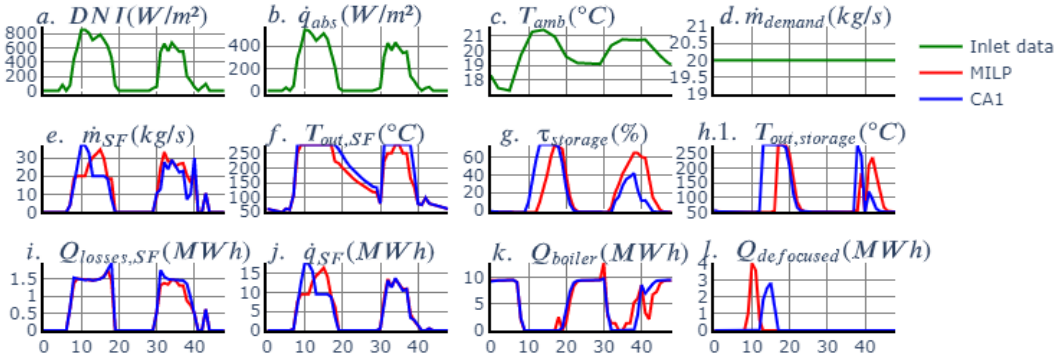


**Fig. 7. Hourly results of the simulation on the 19th and 20th of June**

Fig.7. presents the same variables as in Fig.6, but at a different time of the year, in which irradiation and optical efficiency are higher. Here, the main contribution of the MILP algorithm as compared to CA1 appears in the period of the defocused energy: the MILP algorithm prefers to defocuse in the morning, and then fills the storage to pass the night. Indeed, the MILP algorithm lowers the heat losses of the storage. The maximum filling of the storage is explained by the mass threshold (or temperature threshold) beyond which the storage cannot be charged anymore.

**Discussion**

We can see in Figure 6.h. that the outlet temperature of the storage increases and then decreases: the thermocline is not really a thermocline, the hot/cold zone separation is not clear.

In electricity production, keeping a constant inlet temperature to the turbine is of primary importance, for which it is much more interesting to keep a high quality thermocline. For SHIP with hybridization and a large difference in ΔT between the return and process temperature, it is shown here that it may be advantageous not to favour the quality of the thermocline but rather the quantity of stored energy. There is indeed a loss in exergy because of mixing, but the number of calories from the solar field being higher and the boiler completing the exergy loss most of the time; it appears to be in the end favourable.

Nevertheless, if the SF inlet temperature is close to the SF outlet temperature, the impact of the optimization on the temperature is very small; moreover, the objective in this case should be to keep a thermocline in order to have access to the desired storage temperature. It is highly likely that a parallel architecture of the boiler is more interesting.

5.2. Yearly results

In this section, monthly results are presented over the year.

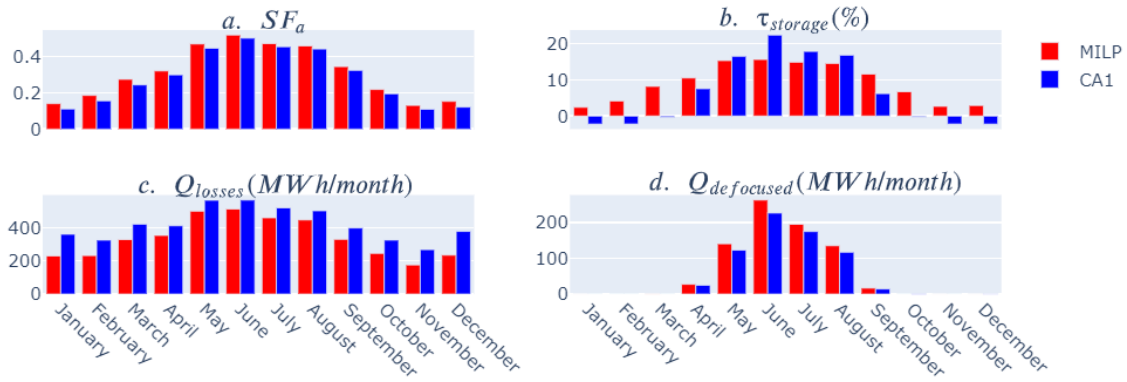


**Fig. 8. Yearly metrics.**

The Solar Fraction ($SF_a$, Fig.8.a.) is calculated as $SF_a = 1 - \frac{Q_{boiler}}{Q_{demand}}$, with $Q_{boiler}$ the heat from the boiler for the month, and $Q_{demand}$ the heat demand during the month. The average charge percentage (Fig.8.b.) is calculated as the hourly average of the charge percentage. The monthly heat losses of the solar field (Fig.8.c.) correspond to the sum of the thermal losses when the solar field is operating. The monthly defocused energy (Fig.8.d.) correspond to the sum of the defocused energy.

The annual solar fraction of the MILP is 30.9% and that of the CA1 approach is 28.5%. During the summer, the two models behave differently: in fact, the MILP prefers to defocus in the morning and to fill the storage later, thus minimizing the thermal losses in the storage. This is why more energy is defocused by the MILP while keeping a higher solar fraction. In winter, the difference is explained by the difference in thermal losses.

## 6. Conclusion

This paper presented the results of a MILP algorithm applied to temperature optimization in a solar field with thermocline storage for industrial process heat. This optimization showed a 2.5%-point increase in the solar fraction as compared to a control trying to reach the process temperature as soon as possible.

Despite the risk of affecting stratification, varying the temperature of the storage inlet, has shown to be interesting in the case of hybridization with a high temperature difference between the return temperature and the process temperature. The use of the storage is maximized by the MILP algorithm, and it is interesting, in the case presented here, not to respect the order imposed by the stratification, because the storage is emptied by the constant demand all night long.

These optimization results seem very interesting, but limited to cases of large temperature difference between the input and the output, which opens a range of optimization. Another dimension of freedom can be found in the case of an industrial site with different heat requirements, and different production sites, approaching the notion of Total Site Analysis. This will be investigated in future works.

## 7. References


Esence, T., Bayón, R., Bruch, A., Rojas, E., 2017. Study of thermocline development inside a dual-media storage tank at the beginning of dynamic processes. Presented at the SOLARPACES 2016: International Conference on Concentrating Solar Power and Chemical Energy Systems, Abu Dhabi, United Arab Emirates, p. 080009. https://doi.org/10.1063/1.4984430

Esence, T., Bruch, A., Fourmigué, J.-F., Stutz, B., 2019. A versatile one-dimensional numerical model for packed-bed heat storage systems. Renewable Energy 133, 190–204. https://doi.org/10.1016/j.renene.2018.10.012

EU SCIENCE HUB, 2017. Photovoltaic Geographical Information System (PVGIS).

Fitsum, B.T., Ramchandra, B., Menegesha, M., 2018. Design Optimization and Demand Side Management of a Solar-Assisted Industrial Heating Using Agent-Based Modelling (ABM): Methodology and Case Study. E3S Web Conf. 64, 02001. https://doi.org/10.1051/e3sconf/20186402001

FriendSHIP, 2021. Deliverable: D1.2 „List of specifications for all components subsystems and global SHIP 200 & SHIP 300 parameters“ – Confidential.

He, G., Chen, Q., Kang, C., Xia, Q., 2016. Optimal Offering Strategy for Concentrating Solar Power Plants in Joint Energy, Reserve and Regulation Markets. IEEE Trans. Sustain. Energy 7, 1245–1254. https://doi.org/10.1109/TSTE.2016.2533637

Hoffmann, J.-F., Fasquelle, T., Goetz, V., Py, X., 2016. A thermocline thermal energy storage system with filler materials for concentrated solar power plants: Experimental data and numerical model sensitivity to different experimental tank scales. Applied Thermal Engineering 100, 753–761. https://doi.org/10.1016/j.applthermaleng.2016.01.110

IEA, 2020. Renewables 2020 - Analysis and forecast to 2025 172.

Ikorotkin, 2019. dae-cpp: A simple but powerful C++ DAE (Differential Algebraic Equation) solver.

Kamerling, S., Vuillerme, V., Rodat, S., 2021. Solar Field Output Temperature Optimization Using a MILP Algorithm and a 0D Model in the Case of a Hybrid Concentrated Solar Thermal Power Plant for SHIP Applications. Energies 14, 3731. https://doi.org/10.3390/en14133731

Moretti, L., Manzolini, G., Martelli, E., 2021. MILP and MINLP models for the optimal scheduling of multi-energy systems accounting for delivery temperature of units, topology and non-isothermal mixing. Applied Thermal Engineering 184, 116161. https://doi.org/10.1016/j.applthermaleng.2020.116161

Okazaki, T., Shirai, Y., Nakamura, T., 2015. Concept study of wind power utilizing direct thermal energy conversion and thermal energy storage. Renewable Energy 83, 332–338. https://doi.org/10.1016/j.renene.2015.04.027

Pousinho, H.M.I., Silva, H., Mendes, V.M.F., Collares-Pereira, M., Pereira Cabrita, C., 2014. Self-scheduling for energy and spinning reserve of wind/CSP plants by a MILP approach. Energy 78, 524–534. https://doi.org/10.1016/j.energy.2014.10.039

Rashid, K., Safdarnejad, S.M., Powell, K.M., 2019. Process intensification of solar thermal power using hybridization, flexible heat integration, and real-time optimization. Chemical Engineering and Processing - Process Intensification 139, 155–171. https://doi.org/10.1016/j.cep.2019.04.004

Wagner, M.J., Gilman, P., 2011. Technical Manual for the SAM Physical Trough Model (No. NREL/TP-5500-51825, 1016437). https://doi.org/10.2172/1016437

Yang, Y., Guo, S., Liu, D., Li, R., Chu, Y., 2018. Operation optimization strategy for wind-concentrated solar power hybrid power generation system. Energy Conversion and Management 160, 243–250. https://doi.org/10.1016/j.enconman.2018.01.040